Fatigue properties of ceramic hollow sphere filled aluminium matrix syntactic foams

Bálint KATONA[a], Gábor SZEBÉNYI[b,c], Imre Norbert ORBULOV[a,c,*]

[a]Department of Materials Science and Engineering, Faculty of Mechanical Engineering, Budapest University of Technology and Economics, Bertalan Lajos utca 7., Budapest, Hungary, 1111

[b]Department of Polymer Engineering, Faculty of Mechanical Engineering, Budapest University of Technology and Economics, Műegyetem rakpart 3., Budapest, Hungary, 1111

[c]MTA–BME Research Group for Composite Science and Technology, Műegyetem rakpart 3., Budapest, Hungary, 1111

*Corresponding author

Address: Department of Materials Science and Engineering, Faculty of Mechanical Engineering, Budapest University of Technology and Economics, Bertalan Lajos utca 7., Budapest, Hungary, 1111

Tel: +36 1 463 2386

Fax: +36 1 463 1366

E-mail: orbulov@eik.bme.hu, orbulov@gmail.com

Abstract

Metal matrix syntactic foams, consisting of two grades of aluminium alloys and a set of oxide ceramic hollow spheres, were investigated in the aspect of cyclic loading. The results of the compressive – compressive cyclic loading with the load asymmetry factor of R=0.1 ensured full reliability design data for the investigated material in the lifetime region, while the fatigue limits were determined by staircase method. Based on the measurements the Wöhler curves of the foams were constructed, including the median curves, their confidence boundaries and the fatigue strength. Regarding the matrix material, the softer matrix ensured higher load levels for the fatigue strength than the more rigid matrix. Considering the size of the reinforcing ceramic hollow spheres, larger spheres performed better than the more vulnerable smaller ones. One common failure mode was isolated for the investigated foams: the samples were broken along a shear band, similar to the case of quasi-static loading.

Keywords: mechanical characterization, composites, porous materials, fatigue

1 Introduction

Metal matrix syntactic foams (MMSFs) consist of a set of hollow spheres (ceramic, metallic or mixed) in metal matrix. The hollow spheres are commercially available in various grades from different suppliers [1-3]. As matrix, usually some kind of lightweight metal is used. MMSFs can be sorted into two subgroups of materials. On one hand they can be mentioned as particle reinforced metal matrix composites (composite metal foams – CMFs), because they contain particle like hollow spheres within the diameter range Ø0.1…10 mm. On the other hand, they can be sorted as cellular materials (foams), due to the hollow nature of the reinforcement.

The basic mechanical properties of MMSFs have been widely studied. The publications focus mainly on the compressive behaviour of the foams (as most common loading mode). Due to its utmost importance the quasi-static compressive test of the metallic foams has been standardized [4, 5]. There are certain research groups, dealing with syntactic foams: for example Fiedler et al. [6-10] have been developed low cost syntactic foams filled by perlite particles. Gupta et al. [11-19] have been investigated various MMSFs, including extremely light, SiC hollow sphere reinforced systems. Lehmhus et al. [17, 20-25] developed high performance MMSFs, based on steels. Skolianos et al. [26] have been interested in powder metallurgy processed MMSFs. Rohatgi et al. [27-33] have been conducted extremely wide range experiments on MMSFs, aiming to characterise their properties in details and to highlight the MMSFs as potential solutions for many industrial applications. Moreover, the wear properties have been investigated and described in [34-41].

The behaviour of MMSFs in cyclic loading is also important, because many applications involve repeated loading. However, only a few publications are available in this field and most of them are focused on 'conventional' open and closed cell foams. In their comprehensive work Ashby et al. addressed the tension, compression and shearing mode fatigue tests of different aluminium foams and gave remarkable suggestions for the test samples geometry and conditions [42], later Degischer and Kriszt summarized some basic aspects based on the available literature [43]. Soubielle et al. investigated ~400 µm pore size replicated aluminium foams in tension-tension loading (R=0.1). The foams displayed cyclic creep coupled with a strong influence of relative density [44]. Amsterdam et al. performed monotonic and cyclic tension tests on closed cell foams produced by powder metallurgy. Tension–tension fatigue tests started with the constant ratchetting of the foam samples followed by an accelerated elongation that lead to failure. [45]. Harte et al. compared the fatigue failure of commercially available open and closed cell aluminium alloy foams in tension-tension and in compression-compression loading. The open cell foam had a relatively uniform microstructure, and underwent homogeneous straining. In contrast, the closed cell foam was more irregular in microstructure, and exhibited a single crush band formed and broadened with additional fatigue cycles [46]. McCullough and Fleck performed cyclic tension and compression tests on closed cell AlMgSi alloy based foams in the relative density range of 0.1-0.4. The fatigue strength of the foams increased with the relative density and the dominant cyclic deformation mode appeared to be material ratchetting [47]. Banhart and Brinkers investigated aluminium-silicon alloy (Al + 7 wt% Si) closed cell foams produced by powder metallurgy (0.5 wt% TiH_2), with different relative densities. The cylindrical specimens were loaded in compression-compression mode. The authors highlighted that the compression strength and the failure criterion were not unambiguous in the case of metallic foams [48]. Pure Al foams with similar structure were tested in cyclic compression by Sugimura et al. A significant novelty in their work was the application of image analysis to record strain maps and to follow the formation and thickening of the deformation bands. The closed cell Al alloys had a relatively well defined fatigue life in cyclic compression, associated with the plastically buckled membranes of the cell walls resulted in a single cyclic deformation band [49]. Zhou and Soboyejo investigated AlMgSi based open cell foams under cyclic compression loading, that resulted in crack nucleation on the surface of the struts. The cracks grew until final failure occurred in the individual struts. In the vicinity of the cracked struts the loads were transferred to the adjacent struts. This led to the acceleration of fatigue damage by formation of macroscopic deformation band(s), resulted in the onset of abrupt strain jumps [50, 51]. Lehmhus et al. investigated powder metallurgy produced Al6061 alloy foams in as foamed and in precipitation hardened condition under cyclic compression-compression loading. The positive effect of precipitation hardening (e. g. the increment in strength values under monotonic loading) was only partially experienced in cyclic loading [52]. The work of Lin

et al. emphasized the application of porous TiNb alloys as bone replacements [50, 51]. The cracks that caused fatigue failure appeared on the surface of the struts in the vicinity of the largest pores [53]. Hakamada et al. focused their work on the cyclic compression tests of closed cell Al foams produced by spacer method using NaCl space holders and a spark plasma sintering equipment. Under cyclic compression the strain increased gradually with cycles and no distinct strain jump was observed for the specimen [54]. Zettl et al. investigated AlMgSi and AlSi alloy based, powder metallurgy produced closed cell foams by ultrasound fatigue testing method under fully reversed tension-compression loading. Preferential areas for crack initiation were initial defects like precracks or holes in the interior sections of cell walls. No strain localization or formation of deformation bands were found and the effect of frequency magnitude found to be negligible within three decades [55, 56]. The effect of sample dimensions, especially of the aspect ratio was investigated by Kim and Kim on closed cell Al-Si-Ca foams. The cyclic compression-compression tests revealed that, the onset of cyclic shortening of foams with lower aspect ratio took place earlier and the fatigue strength was lower compared to the specimens with higher aspect ratio [57]. Kolluri et al. performed cyclic compression-compression tests at constant stress amplitude levels on closed-cell Al foam in laterally constrained and unconstrained condition. The results showed that while the early stages of strain accumulation due to fatigue loading were independent of constraint, the rapid strain accumulation stages behaviour were sensitive to the constraint [58]. One step further, sandwich beams (with Al alloy foam core) were also tested in cyclic four-point-bending by Harte et al. The combined experimental and theoretical study showed that a reduction in the strength of sandwich beams existed for cyclic loading compared to monotonic loading [59]. Moreover, Schultz et al. investigated foams in the aspect of potential helicopter components [60].

As it is presented above, the different research groups published results about versatile foam systems and different cyclic loadings. Most of the investigations apply R=0.1 stress asymmetry factor, but the test frequencies can differ significantly. On the other hand, MMSFs have been not mentioned yet. The only similar work on CMFs that contain steel hollow spheres in aluminium matrix (made by gravity casting) or in steel matrix (made by powder metallurgy method) was published by Vendra et al. Under cyclic compression loading, the CMFs showed high cyclic stability and the deformation of the composite foam samples could be divided into three stages – linear increase in strain with fatigue cycles (stage I), minimal strain accumulation in large number of cycles (stage II) and rapid strain accumulation within few cycles up to complete failure (stage III). The deformation of the MMSFs occurred to be uniform compared to regular metal foams, which deform by forming collapse bands at weaker sections [61].

The aim of this paper is to widen the fatigue properties datasets available for the compression-compression loading of MMSFs by the investigation of Al99.5 and AlSi12 matrix MMSFs with different filler materials.

2 Materials and methods

Al99.5 and AlSi12 alloys were applied as matrix materials, their chemical compositions are listed in Table 1. As filler, Globocer (GC) grade ceramic hollow spheres were applied, provided by Hollomet GmbH. [1]. The material of the hollow spheres consists of 38 wt% Al_2O_3, 43 wt% SiO_2 and 19 wt% $3Al_2O_3 \cdot 2SiO_2$. The hollow spheres follow a normal distribution regarding their diameter (1425±42 µm) and wall thickness (60±1.7 µm), while their density is 0.816 gcm^{-3}. The amount of the filler material was maintained at ~65 vol%, ensured by gentle tapping and knocking during the filling process [62, 63]. The MMSFs were produced by pressure infiltration. During the infiltration 400 kPa infiltration pressure was applied for the infiltration time of 30 s. The infiltration temperature was always set to 50°C above the melting temperature of the matrix materials (660°C for Al99.5 and 575°C for AlSi12). The infiltration pressure was significantly larger than the threshold pressure of the hollow spheres, therefore the amount of un-infiltrated voids could be neglected (please refer to the micrographs in sections 3.1 and 3.2). However, due to the nature of the pressure infiltration and because of the uneven wall thickness of the hollow spheres, the infiltration pressure may have exceeded the crush strength of a few hollow spheres. In these cases, the spheres were infiltrated (less than 3 vol% of the spheres). The infiltration process is described in details elsewhere [64-66]. The produced foams were designated after their constituents, for example Al99.5-GC stands for an MMSF sample with Al99.5 matrix and ~65 vol% of Globocer filler material. Cylindrical samples with diameter of Ø8.5 mm and height of 12.75 mm (1.5 aspect ratio) were machined from the produced blocks.

Table 1. Chemical composition of the matrix materials (in wt%)

Matrix	Si	Fe	Mn	Mg	Cu	Zn	Al
Al99.5	0.250	0.400	0.050	0.050	0.050	0.050	rem.
AlSi12	12.830	0.127	0.005	0.010	0.002	0.007	rem.

For classic fatigue tests, load levels (k) should be determined, that describe the maximum load (σ_{max}) during each fatigue cycle in a relation to a limit strength. In the case of conventional metals, the load levels are usually related to the proof strength ($R_{p0.2}$) that is measured by simple tensile tests. In the case of MMSFs the proof strength can be substituted by the compressive strength (σ_c, the first local maximum in the engineering compressive stress – strain diagram, that causes irreversible failure, see Fig. 1).

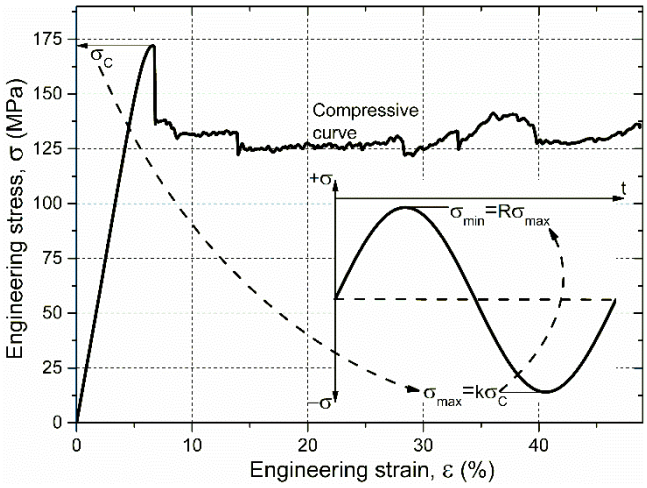

Fig. 1 Typical quasi-static compressive curve of MMSFs and the derivation of the cyclic loading parameters σ_{min} and σ_{max} (inset figure)

The compressive strength (σ_c) of the foams, was measured for each material type on six samples (Table 2). On this basis, the load levels can be defined as the ratio of the maximal load and the compressive strength within the loading cycle (Eq. 1). The load level expresses similar load intensity, for the investigated materials that may have different compressive strength.

$$k = \frac{\sigma_{max}}{\sigma_C} 100\ (\%) \qquad \text{Eq. 1}$$

In our case the load level was altered between 60-100%. Fatigue tests were performed on an Instron 8872 type closed loop servo-hydraulic testing machine under force control and in compression-compression mode (stress asymmetry factor of $R=0.1$). The frequency of the fatigue tests was set to $f=10$ Hz and the load form followed a sine curve (inset of Fig. 1). The cylindrical specimens were carefully lubricated and placed between hardened and polished plates in a four column upsetting tool. The overall deformation of the specimens was measured by a strain gage as a function of cycles. In order to get information about the reliability of the test sequences the percent replication (PR) has been calculated (Eq. 2).

$$PR = \left(1 - \frac{N_K}{N_S}\right) 100 \qquad \text{Eq. 2}$$

Where N_K is the number of load levels and N_S is the overall number of the specimens. PR between 17-33% corresponds to preliminary and exploratory tests, PR=34-50% is for research and development tests, PR=50-75% is for design allowable tests, while full reliability data tests requires PR=76% or higher [67]. The PR values are listed in Table 2, all test sequences satisfy the strictest reliability criterion.

Table 2 Compressive strength, sample number and reliability data

Foam	Compressive strength, σ_c (MPa)	Number of samples at load level			Reliability, PR (%)	SUM
		k=80%	k=85%	k=90%		
Al99.5-GC	19.7	3	9	9	85.7	
AlSi12-GC	40.0	9	9	9	88.9	
Overall number of samples		12	18	18		48
Overall number of cycles		6966673	28377	3320		6998370
Overall duration of tests (hours)		193.52	0.79	0.09		194.40

3 Results and discussion

3.1 Fatigue properties

During the fatigue tests, the maximum values of the compressive engineering deformation were recorded in the function of cycles (Fig. 2). The curves can be divided into three parts [61] (see Fig. 3). In stage I, the strain increases sharply up to a small value after a small number of cycles. Next, the strain remains relatively constant over a large number of cycles (stage II). This stage is known as incubation period [49]. A higher load ratio increases the overall strain in stage II. Stage III is accompanied by densification of the material and a rapid strain accumulation after a critical number of cycles. Higher load ratios shift the onset of stage III towards lower numbers of cycles.

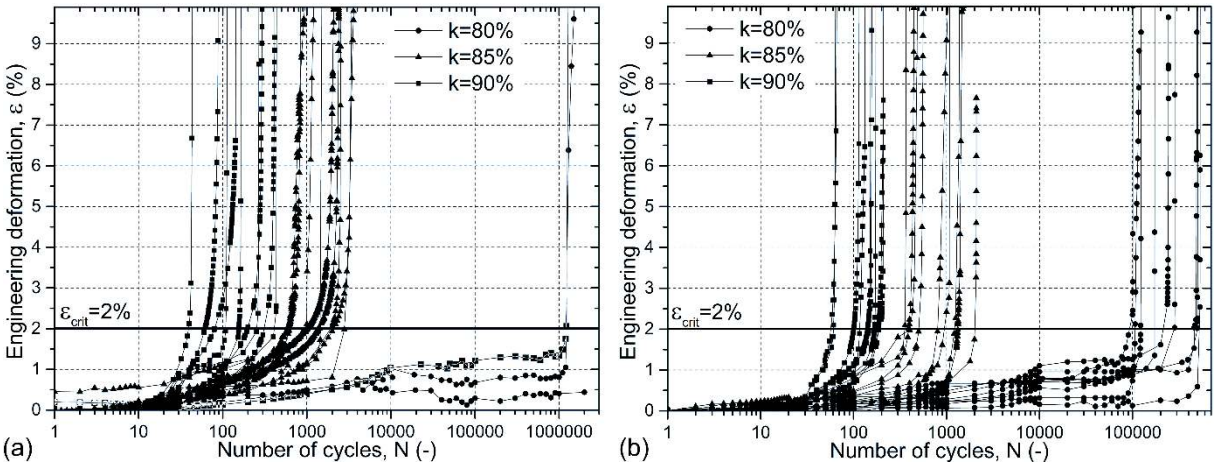

Fig. 2 The measured compressive engineering deformation – number of cycles curves of (a) Al99.5-GC and (b) AlSi12-GC

For further investigation of the deformation mechanism the (idealised) deformation rate is plotted in Fig. 3b in the function of the cycles. In the first section the initial plastic deformation in the weakest struts occurs, and due to the hardening of the material the deformation rate decreases. In the second, incubation part the deformation rate is almost constant and near to zero, finally in the last part rapid damage accumulation takes place and the deformation rate increases steeply.

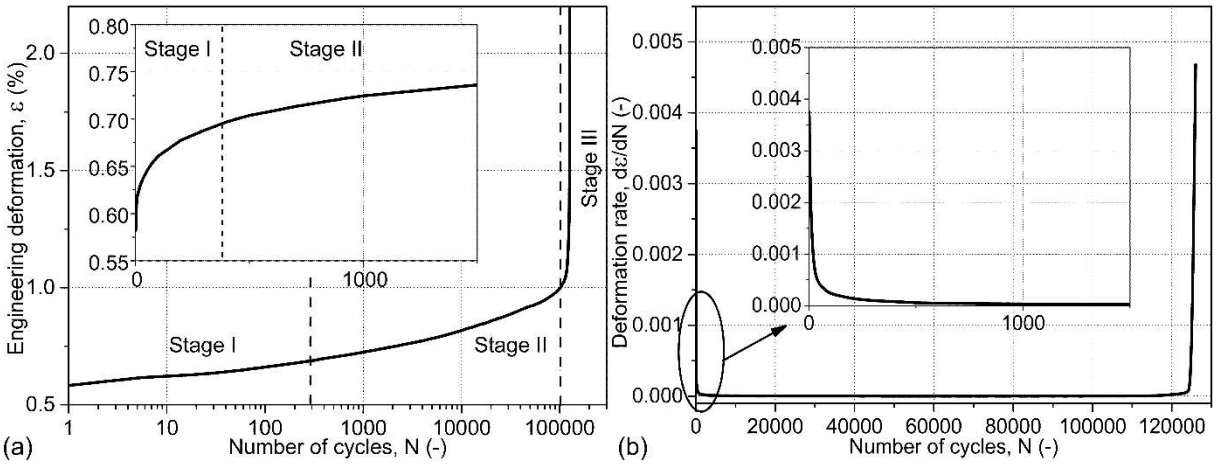

Fig. 3 The idealised compressive engineering deformation (a) and engineering deformation rate (b) in the function of cycles

For the correct evaluation of the deformation – cycle curves a failure criterion needs to be defined, that always depends on the desired application. As there is no conventional criterion limit for the failure [48], the obtained deformation – number of cycle curves were evaluated at an arbitrarily chosen $\varepsilon_{crit}=2\%$ (Fig. 2a) in order to get the failure cycles (N_F). It should be emphasized that $\varepsilon_{crit}=2\%$ engineering deformation corresponds to a macroscopically observable failure in the specimen. The obtained failure cycles showed large scatter, as it is usual in the case of fatigue tests, therefore mathematical statistics, namely the Weibull distribution function (Eq. 3) was used to determine the expected number of cycles up to failure at a survival level (or probability, P_S) of 50%.

$$P_S = 1 - e^{-\left(\frac{N-N_0}{\alpha}\right)^{\beta}} \quad \text{(Eq. 3)}$$

Where N is the independent variable, for which the equation should be evaluated to get the number of cycles up to the failure, N_0 is the threshold parameter, α is the scale parameter while β is the shape parameter of the function. During the evaluation, the number of cycles up to the failure (N_F) at the investigated load level should be sorted into ascending order. In the next step a Median Rank (MR) value should be assigned to each number of cycles up to the failure. The expression of the median rank is in Eq. 4.

$$MR = \frac{i-0.3}{n+0.4} \quad \text{(Eq. 4)}$$

Where i is the number of the current point and n is the sample number on the given load level. For example in the case of a $n=9$ element sample set the MR value of the $i=5^{th}$ sample is $MR=0.5$. Subsequently, Eq. 3 should be fitted on the N_F–MR points to obtain the parameters of Eq. 3 and finally the equation (Eq. 3.) should be solved for N. An example of the Weibull fitting is shown in Fig. 4.

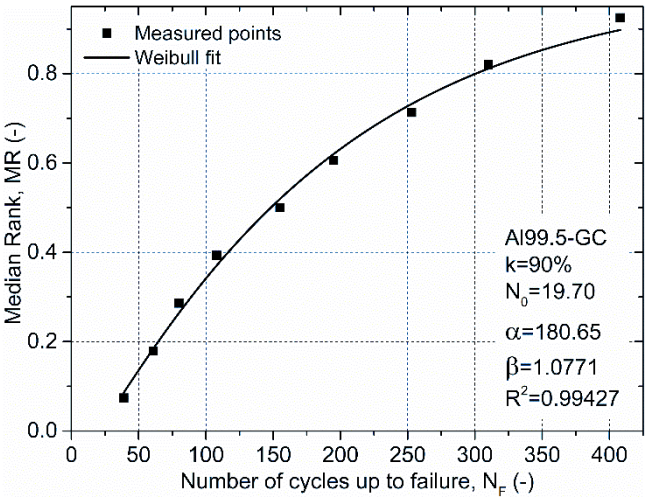

Fig. 4 Weibull fitting example for Al99.5-GC foam at k=90%

The next step is to construct the Wöhler-curve of the materials, that consists of two main parts. The first, endurance (or finite lifetime) part establish a relationship between the load level and the expected lifetime of the material. The second part represents the fatigue strength of the material. Considering the first part, the above derived results of the described mathematical statistic method are valid for the endurance range and the fitted line on them represents the endurance part of the Wöhler-curve. By using this curve in the case of a given part and a given loading, the expected lifetime of the part can be predicted at the 50% survival probability (P_S). Regarding the second part, the load level corresponds to the fatigue strength can be determined by the staircase method [67]. First, the load level corresponds to the mean fatigue limit has to be estimated, and a fatigue life test has to be conducted at a little higher load level than the estimated mean. If the specimen fails prior to the life of interest ($2 \cdot 10^6$ cycles in our case), the next specimen has to be tested at a somewhat lower load level. If the specimen does not fail within this life of interest, a new test has to be conducted at a higher stress level. Therefore, each test depends on the previous test result, and the test series continues with a load level increased or decreased. The load level increments are usually taken to be less than about 5% of the initial estimate of the mean [68]. Tables 3 and 4 represent the data for the staircase method in the case of the investigated MMSFs, while Figs. 5a and 5b represent the results of the measurements for the Al99.5 and AlSi12 matrix MMSFs, respectively.

Table 3 The data of the staircase method for the Al99.5-GC syntactic foams

Foam	Compressive strength, σ_c (MPa)	Number of samples at load level				SUM
		k=0.7625	k=0.775	k=0.7875	k=0.80	
Al99.5-GC	19,7	1	2	3	3	9
Overall number of cycles		2000000	3292151	5142563	4395000	14829714
Overall duration of tests (hours)		55.56	91.44	142.84	12.21	302.05

Table 4 The data of the staircase method for the AlSi12-GC syntactic foams

Foam	Compressive strength, σ_c (MPa)	Number of samples at load level			SUM
		k=0.725	k=0.7375	k=0.75	
AlSi12-GC	40,0	2	4	3	9
Overall number of cycles		4000000	5292984	3647600	12940584
Overall duration of tests (hours)		111.11	147.03	101.32	359.46

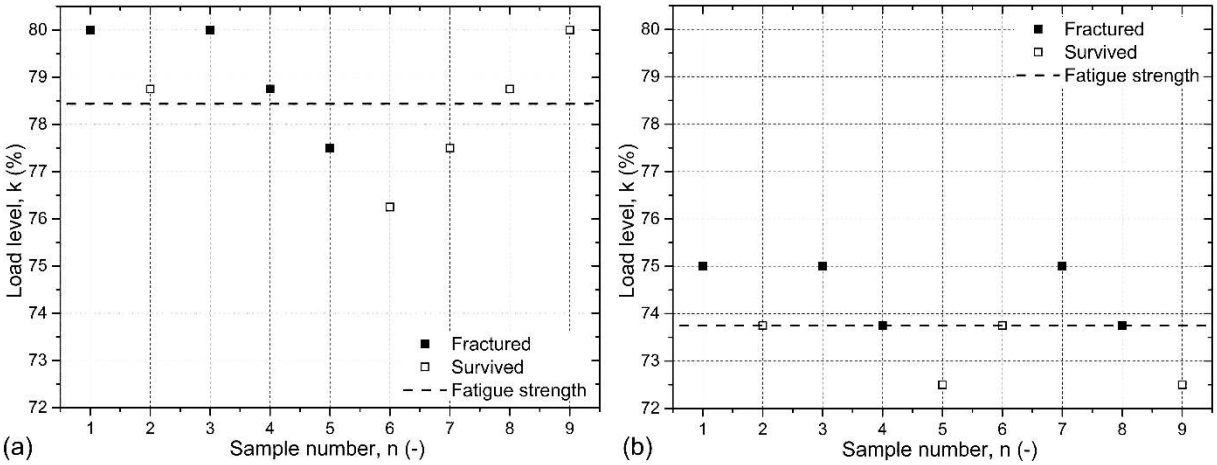

Fig. 5 Results of the staircase method for Al99.5-GC (a) and AlSi12-GC (b) MMSFs

The staircase method resulted in the load levels of 78.44% and 73.75%, that corresponds to the fatigue strength of 15.45 MPa and 29.50 MPa for the Al99.5-GC and AlSi12-GC MMSFs, respectively. In the possession of the finite lifetime data and fatigue limit it is possible to construct the Wöhler-curves of the MMSFs (Fig. 6). In Fig. 6 the measured points are shown by hollow squares, while the evaluated points are designated by black squares. The endurance part starts from k=100% as that corresponds to a single (1/4 cycle) uploading to the compressive strength. In the finite lifetime region, the black line was fitted on the evaluated points by the least square method (R^2=0.976 and R^2=0.978 for the Al99.5-GC and AlSi12-GC foams, respectively). The load levels corresponding to the fatigue limits and obtained by the staircase method are also plotted by black lines in the diagrams. The finite lifetime regions are supplemented by 90% reliability bands at 95% confidence level according to the ruling ASTM method (black dashed lines) [67]. Considering the identical scales and comparing Figs. 6a and 6b the technical purity Al99.5 matrix material ensured higher fatigue limit and higher lifetimes for a given load level. This phenomenon can be explained by the more or less pronounced rigidity of the high Si content eutectic Al matrix and by the presence of the Si lamellae in the matrix, resulting in a moderate stress concentrating effect. On the other hand, the more ductile and soft technical purity Al matrix could hinder the incidental crack propagations, resulting in a higher lifetime. These curves can be directly used to predict the expected lifetime of the MMSF parts based on their maximum permitted loading during operation, that could be determined by measurements on actual parts or can be estimated by finite element methods.

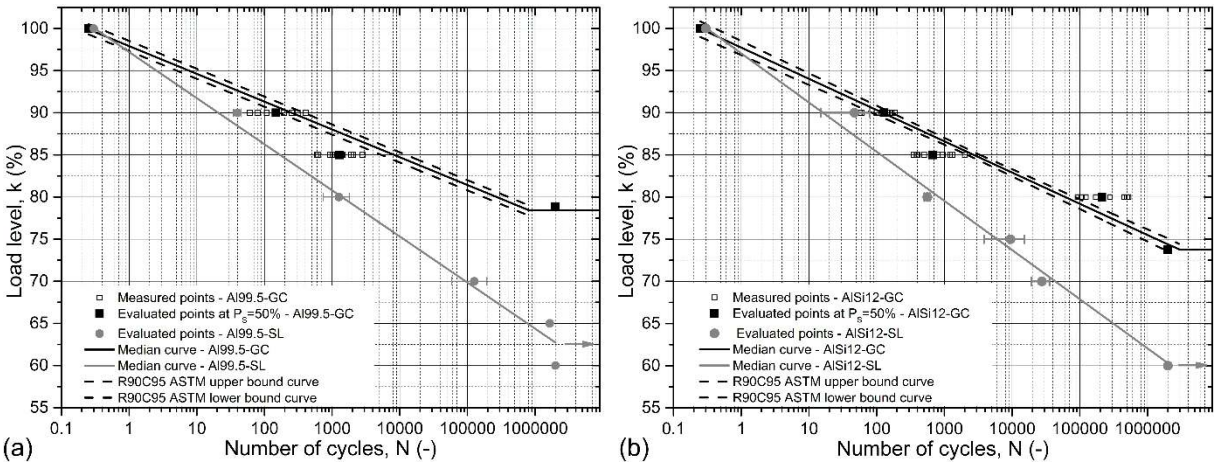

Fig. 6 Wöhler-curve for Al99.5-GC (a) and AlSi12-GC (b) MMSFs

For comparison and to investigate the size effect of the hollow spheres preliminary measurements on MMSFs reinforced by smaller hollow spheres with identical chemical composition were performed. The smaller hollow spheres are commercially available under the SL300 grade name (provided by Envirospheres Pty. Ltd. [2], designated by SL in the diagrams). The average diameter (150±4.1 µm) and wall thickness (6.75±0.2 µm) of the smaller, SL grade hollow spheres were about one tenth of the GC grade spheres, while their density was slightly lower (0.691 gcm^{-3}). The preliminary tests were performed on fewer samples and the results were evaluated by simpler statistics (average and scatter). However, two important trends can be clearly observed: (i) in the case of the smaller hollow spheres similar relationship can be seen regarding the matrix material: the softer Al99.5 matrix ensured higher expected lifetimes at certain load levels and (ii) the lifetime region of the smaller spheres always run well below the curves of the GC spheres. This can be explained by the different failure mechanism of the hollow spheres. The smaller SL spheres have thinner walls in which any defect can easily be the starting point of a crack (Fig. 7). In Fig. 7 two cracks are highlighted by white ellipses. The first one has a horizontal direction that is perpendicular to the compressive loading and therefore moderately dangerous, because the compressive loading tends to close this crack. The second one is vertical and due to the additional radial forces awakened by the compressive loading and the resistance of the material against deformation, this crack is in opening mode and therefore can propagate into the matrix as it can be seen in Fig. 7b in magnified view.

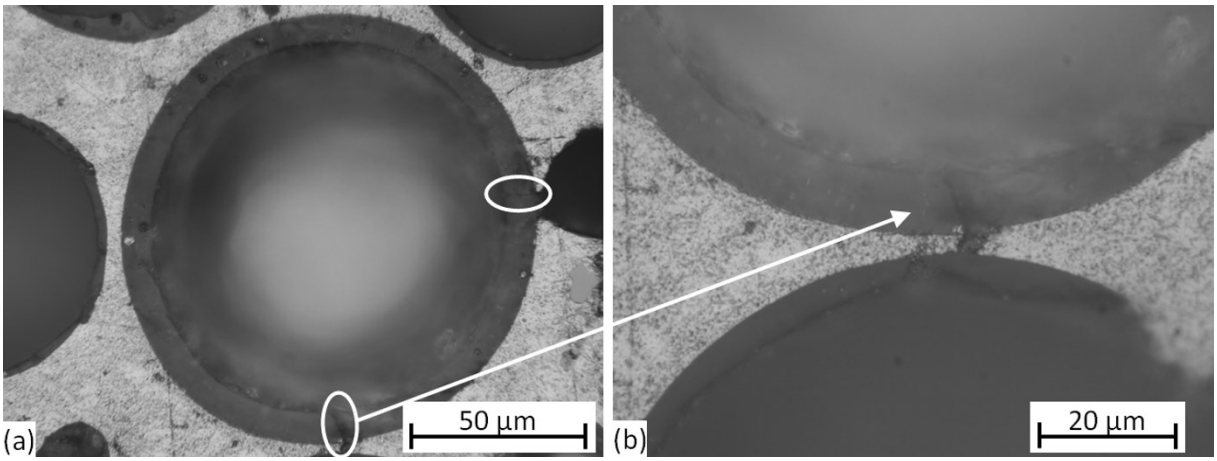

Fig. 7 SL grade hollow sphere in Al99.5 matrix (a) and magnified view of a crack (b)

Moreover, the smaller hollow spheres are situated closer to each other, therefore the cracks have to run smaller distances in the relatively soft and ductile matrix material to reach the next rigid ceramic hollow sphere (Fig. 7b). Thus a shearing plane can be easily initiated (Fig. 8) and in this way, the crack propagation can be faster than in the case of larger, GC grade reinforcement.

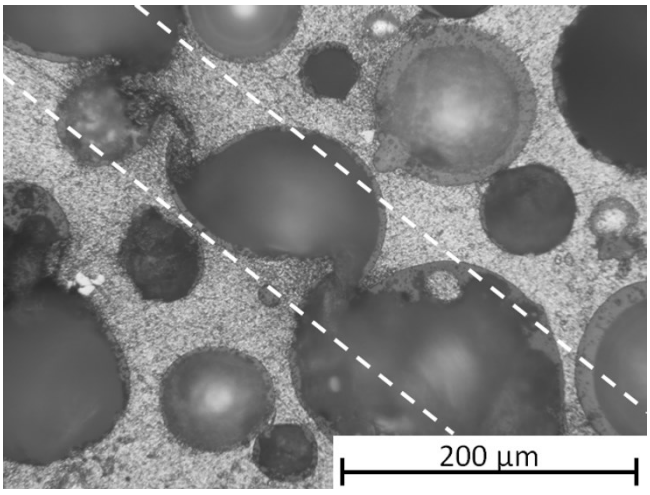

Fig. 8 Crack plane formed by the propagation of cracks between closely situated SL spheres in Al99.5-SL foam

3.2 Failure mechanism

After the fatigue tests the failed specimens were investigated by optical microscopy to map the failure mechanism of the materials. All of the investigated materials failed very similar to their quasi-static compressive fracture mechanism [69, 70]. During the cyclic loading the matrix suffered small amount of plastic deformation and subsequently a shear band formed, closing ~30-40° to the direction of the compressive load. The initiation of the cleavage band depends on the crush strength of the hollow spheres. The typical failure of the material is shown in Fig. 9.

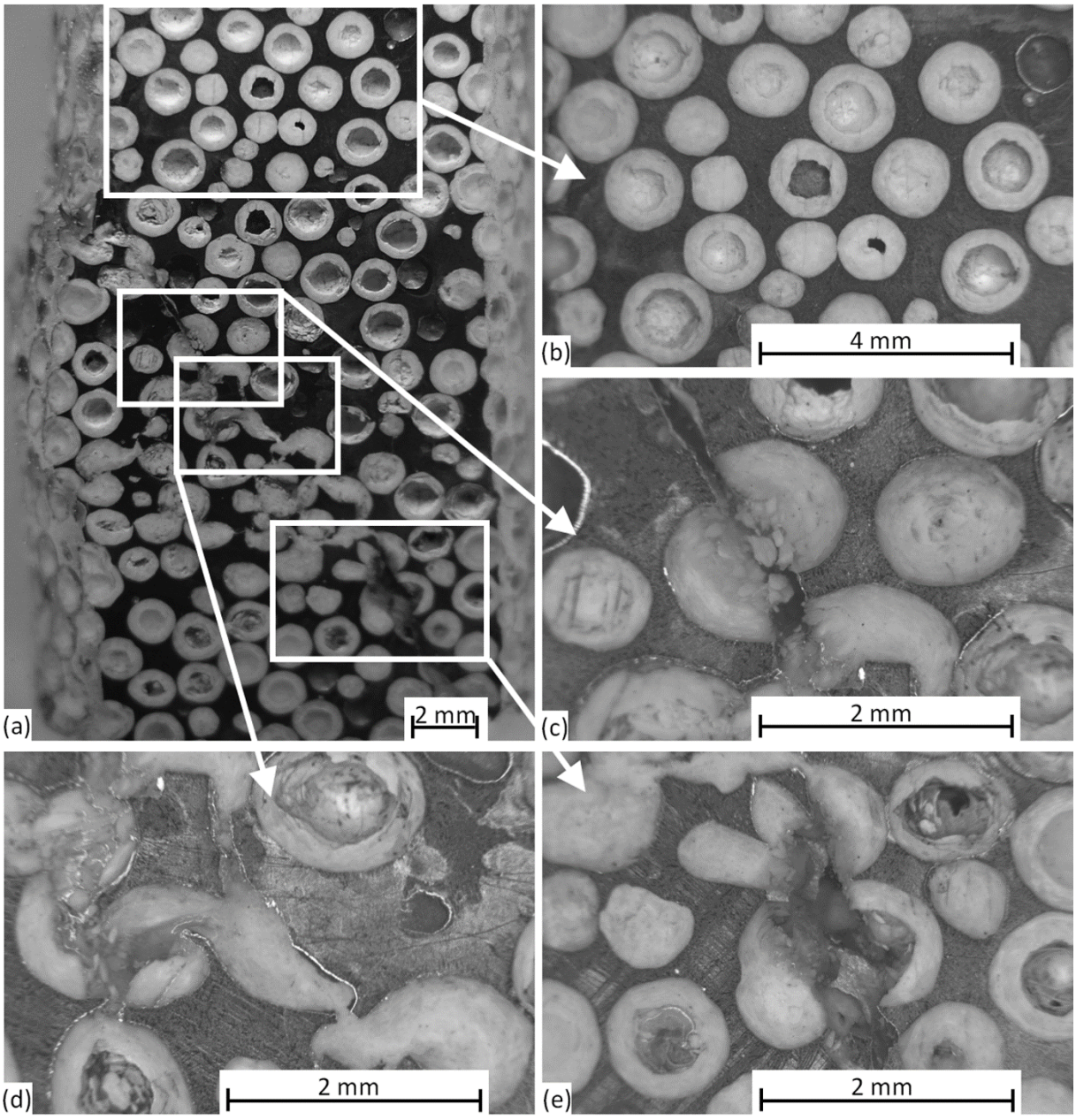

Fig. 9 Typical failure of GC grade hollow sphere reinforced foams (a) macrograph of the whole specimen, (b-e) micrographs about the vicinity of the shear band

Fig. 9a shows the entire specimen, ground almost to its half in order to reveal the presence of the shear band, that is clearly observable across the whole section of the sample. Despite the presence of the sheared zone, the upper part of the sample is unharmed as it is shown in Fig. 9b. This fact emphasizes one of the most important properties of the MMSFs, namely its high damage tolerance. Far from the shear band the hollow spheres remained unharmed and ready to act against further loading. Figs. 9c-e present the vicinity of the shear band (the band appeared in the direction of the maximal shear loading). Within the shear band the hollow spheres are completely broken into halves

and slid on each other. The neighbouring spheres are also broken, but one or two spheres farther they are intact and unharmed. These hollow spheres can also bear further loading. This failure mechanism has been also observed and confirmed by Luong et al. [71]. In Al – SiC hollow sphere systems Luong et al. highlighted the failure of weak hollow spheres at the peak stress. Some of the appeared cracks could propagate to the matrix material. Along the weakest hollow spheres, the shear band formation in the matrix lead to the major failure activity. Parts of the broken hollow spheres are compacted in their own cavity and the materials densified [71].

4 Conclusions

From the above detailed investigations and analysis of the MMSFs, the following conclusions can be drawn:

- The Wöhler-curve of the hollow sphere reinforced MMSFs were constructed according to the ruling ASTM standard for the case of compressive cyclic loading. The results include the median curves, their 95% confidence boundaries and the fatigue strength.
- The softer, technical purity Al99.5 matrix ensured higher load levels for the fatigue strengths than the more rigid, eutectic AlSi12 matrix.
- Regarding the size of the reinforcing ceramic hollow spheres, the larger, GC grade spheres performed better, because the smaller spheres are more vulnerable and the cracks have to propagate shorter distances within the ductile matrix to the next rigid ceramic sphere.
- Considering the failure mechanism of the investigated MMSFs, one common failure mode was isolated: the samples were broken along a shear band, similar to the case of quasi-static loading. The hollow spheres within and near to the shear band were broken into halves and slid on each other along the shear plane, however the spheres far from the shear band remained unharmed and could withstand further loading.

Acknowledgements

This paper was supported by the János Bolyai Research Scholarship of the Hungarian Academy of Sciences (Imre Norbert ORBULOV, Gábor SZEBÉNYI).

References

[1] Hollomet GmbH
https://web.archive.org/web/20161003134821/http://www.hollomet.com/home.html, last accessed: 3rd October 2016.
[2] Envirospheres Ltd.
https://web.archive.org/web/20161003134943/http://www.envirospheres.com/products.asp, last accessed: 3rd October 2016.

[3] Deep Springs Technology
https://web.archive.org/web/20161003135022/http://teamdst.com/pdf/HollowShells_MTG119-A%20Web.pdf, last accessed: 3rd October 2016.
[4] DIN 50134 Testing of metallic materials - Compression test of metallic cellular materials (2008).
[5] ISO 13314 Mechanical testing of metals - Ductility testing - Compression test for porous and cellular materials (2011).
[6] M. Taherishargh, I.V. Belova, G.E. Murch, T. Fiedler, Low-density expanded perlite–aluminium syntactic foam, Mater. Sci. Eng. A. 604 (2014) 127-134.
[7] M. Taherishargh, I.V. Belova, G.E. Murch, T. Fiedler, On the mechanical properties of heat-treated expanded perlite–aluminium syntactic foam, Mater. Des. 63 (2014) 375-383.
[8] M. Taherishargh, I.V. Belova, G.E. Murch, T. Fiedler, Pumice/aluminium syntactic foam, Mater. Sci. Eng. A 635 (2015) 102-108.
[9] M. Taherishargh, M.A. Sulong, I.V. Belova, G.E. Murch, T. Fiedler, On the particle size effect in expanded perlite aluminium syntactic foam, Mater. Des. 66 (2015) 294-303.
[10] T. Fiedler, M. Taherishargh, L. Krstulović-Opara, M. Vesenjak, Dynamic compressive loading of expanded perlite/aluminum syntactic foam, Mater. Sci. Eng. A 626 (2015) 296-304.
[11] N. Gupta, A functionally graded syntactic foam material for high energy absorption under compression, Mater. Lett. 61 (2007) 979-982.
[12] N. Gupta, R. Maharsia, H. Dwayne Jerro, Enhancement of energy absorption characteristics of hollow glass particle filled composites by rubber addition, Mater. Sci. Eng. A 395 (2005) 233-240.
[13] N. Gupta, V.C. Shunmugasamy, High strain rate compressive response of syntactic foams: Trends in mechanical properties and failure mechanisms, Mater. Sci. Eng. A 528 (2011) 7596-7605.
[14] N. Gupta, E. Woldesenbet, P. Mensah, Compression properties of syntactic foams: effect of cenosphere radius ratio and specimen aspect ratio, Composites Part A 35 (2004) 103-111.
[15] D.D. Luong, N. Gupta, A. Daoud, P.K. Rohatgi, High strain rate compressive characterization of aluminum alloy/fly ash cenosphere composites, JOM 63 (2011) 53-56.
[16] D.D. Luong, N. Gupta, P.K. Rohatgi, The high strain rate compressive response of Mg-Al alloy/fly Ash cenosphere composites, JOM 63 (2011) 48-52.
[17] D.D. Luong, V.C. Shunmugasamy, N. Gupta, D. Lehmhus, J. Weise, J. Baumeister, Quasi-static and high strain rates compressive response of iron and Invar matrix syntactic foams, Mater. Des. 66 (2015) 516-531.
[18] P.K.R. Nikhil Gupta, Metal Matrix Syntactic Foams, DEStech Publications, Inc,, Lancaster, Pennsylvania, USA, 2014.
[19] G.A. Rocha Rivero, B.F. Schultz, J.B. Ferguson, N. Gupta, P.K. Rohatgi, Compressive properties of Al-A206/SiC and Mg-AZ91/SiC syntactic foams, J. Mater. Res. 28 (2013) 2426-2435.
[20] D. Lehmhus, J. Weise, J. Baumeister, L. Peroni, M. Scapin, C. Fichera, M. Avalle, M. Busse, Quasi-static and Dynamic Mechanical Performance of Glass Microsphere- and Cenosphere-based 316L Syntactic Foams, Proc. Mater. Sci. 4 (2014) 383-387.
[21] L. Peroni, M. Scapin, M. Avalle, J. Weise, D. Lehmhus, Dynamic mechanical behavior of syntactic iron foams with glass microspheres, Mater. Sci. Eng. A 552 (2012) 364-375.
[22] L. Peroni, M. Scapin, M. Avalle, J. Weise, D. Lehmhus, J. Baumeister, M. Busse, Syntactic Iron Foams - On Deformation Mechanisms and Strain-Rate Dependence of Compressive Properties, Adv. Eng. Mater. 14 (2012) 909-918.

[23] L. Peroni, M. Scapin, C. Fichera, D. Lehmhus, J. Weise, J. Baumeister, M. Avalle, Investigation of the mechanical behaviour of AISI 316L stainless steel syntactic foams at different strain-rates, Composites Part B 66 (2014) 430-442.
[24] J. Weise, D. Lehmhus, J. Baumeister, R. Kun, M. Bayoumi, M. Busse, Production and Properties of 316L Stainless Steel Cellular Materials and Syntactic Foams, Steel Res. Int. 85 (2014) 486-497.
[25] J. Weise, N. Salk, U. Jehring, J. Baumeister, D. Lehmhus, M.A. Bayoumi, Influence of Powder Size on Production Parameters and Properties of Syntactic Invar Foams Produced by Means of Metal Powder Injection Moulding, Adv. Eng. Mater. 15 (2013) 118-122.
[26] C.A. Vogiatzis, A. Tsouknidas, D.T. Kountouras, S. Skolianos, Aluminum–ceramic cenospheres syntactic foams produced by powder metallurgy route, Mater. Des. 85 (2015) 444-454.
[27] J.B. Ferguson, J.A. Santa Maria, B.F. Schultz, P.K. Rohatgi, Al–Al2O3 syntactic foams—Part II: Predicting mechanical properties of metal matrix syntactic foams reinforced with ceramic spheres, Mater. Sci. Eng. A 582 (2013) 423-432.
[28] J.A.S. Maria, B.F. Schultz, J.B. Ferguson, P.K. Rohatgi, Al-Al2O3 Syntactic Foams – Part I: Effect of matrix strength and hollow sphere size on the quasi-static properties of Al-A206/Al2O3 syntactic foams, Mater. Sci. Eng. A 582 (2013) 415-422.
[29] P.K. Rohatgi, A. Daoud, B.F. Schultz, T. Puri, Microstructure and mechanical behavior of die casting AZ91D-Fly ash cenosphere composites, Composites Part A 40 (2009) 883-896.
[30] P.K. Rohatgi, R.Q. Guo, H. Iksan, E.J. Borchelt, R. Asthana, Pressure infiltration technique for synthesis of aluminum–fly ash particulate composite, Mater. Sci. Eng. A 244 (1998) 22-30.
[31] P.K. Rohatgi, N. Gupta, S. Alaraj, Thermal expansion of aluminum-fly ash cenosphere composites synthesized by pressure infiltration technique, J. Compos. Mater. 40 (2006) 1163-1174.
[32] P.K. Rohatgi, N. Gupta, B.F. Schultz, D.D. Luong, The synthesis, compressive properties, and applications of metal matrix syntactic foams, JOM 63 (2011) 36-42.
[33] J.A. Santa Maria, B.F. Schultz, J.B. Ferguson, N. Guptan, P.K. Rohatgi, Effect of hollow sphere size and size distribution on the quasi-static and high strain rate compressive properties of Al-A380-Al2O3 syntactic foams, J. Mater. Sci. 49 (2014) 1267-1278.
[34] N. Jha, A. Badkul, D.P. Mondal, S. Das, M. Singh, Sliding wear behaviour of aluminum syntactic foam: A comparison with Al–10wt% SiC composites, Tribology Int. 44 (2011) 220-231.
[35] K. Májlinger, B. Bozóki, G. Kalácska, R. Keresztes, L. Zsidai, Tribological properties of hybrid aluminum matrix syntactic foams, Tribology Int. 99 (2016) 211-223.
[36] D.P. Mondal, S. Das, N. Jha, Dry sliding wear behaviour of aluminum syntactic foam, Mater. Des. 30 (2009) 2563-2568.
[37] M. Ramachandra, K. Radhakrishna, Effect of reinforcement of flyash on sliding wear, slurry erosive wear and corrosive behavior of aluminium matrix composite, Wear 262 (2007) 1450-1462.
[38] M. Ramachandra, K. Radhakrishna, Synthesis-microstructure-mechanical properties-wear and corrosion behavior of an Al-Si (12%)-Flyash metal matrix composite, J. Mater. Sci. 40 (2005) 5989-5997.
[39] P.K. Rohatgi, R.Q. Guo, Mechanism of abrasive wear of Al-Si hypoeutectic alloy containing 5 vol% fly ash, Tribology Lett. 3 (1997) 339-347.
[40] V. Saravanan, P.R. Thyla, S.R. Balakrishnan, The dry sliding wear of cenosphere-aluminium metal matrix composite, Adv. Compos. Lett. 23 (2014) 49-58.
[41] K. Májlinger, Wear properties of hybrid AlSi12 matrix syntactic foams, Int. J. Mater. Res. 106 (2015) 1165-1173.

[42] M. Ashby, A.G. Evans, N.A. Fleck, L.J. Gibson, J.W. Hutchinson, H.N.G. Wadley, Metal Foams: A Design Guide, Butterwort- Heinemann, Madras, 2000.
[43] H.P. Degischer, B. Kriszt, Handbook of cellular metals: production, processing, applications, Wiley-VCH2002.
[44] S. Soubielle, L. Salvo, F. Diologent, A. Mortensen, Fatigue and cyclic creep of replicated microcellular aluminium, Mater. Sci. Eng. A 528 (2011) 2657-2663.
[45] E. Amsterdam, J.T.M. De Hosson, P.R. Onck, Failure mechanisms of closed-cell aluminum foam under monotonic and cyclic loading, Acta Mater. 54 (2006) 4465-4472.
[46] A.M. Harte, N.A. Fleck, M.F. Ashby, Fatigue failure of an open cell and a closed cell aluminium alloy foam, Acta Mater. 47 (1999) 2511-2524.
[47] McCullough, Fleck, The stress–life fatigue behaviour of aluminium alloy foams, Fatigue Fract. Eng. Mater. Struct. 23 (2000) 199-208.
[48] J. Banhart, W. Brinkers, Fatigue Behavior of Aluminum Foams, J. Mater. Sci. Lett. 18 (1999) 617-619.
[49] Y. Sugimura, A. Rabiei, A.G. Evans, A.M. Harte, N.A. Fleck, Compression fatigue of a cellular Al alloy, Mater. Sci. Eng. A 269 (1999) 38-48.
[50] J. Zhou, W.O. Soboyejo, Compression–compression fatigue of open cell aluminum foams: macro-/micro- mechanisms and the effects of heat treatment, Mater. Sci. Eng. A 369 (2004) 23-35.
[51] J. Zhou, Z. Gao, A.M. Cuitino, W.O. Soboyejo, Fatigue of As-Fabricated Open Cell Aluminum Foams, J. Eng. Mater. Techn. 127 (2005) 40-45.
[52] D. Lehmhus, C. Marschner, J. Banhart, H. Bomas, Influence of heat treatment on compression fatigue of aluminium foams, J. Mater. Sci. 37 (2002) 3447-3451.
[53] J.-g. Lin, Y.-f. Zhang, M. Ma, Preparation of porous Ti35Nb alloy and its mechanical properties under monotonic and cyclic loading, Trans. Nonferrous Metals Soc. China 20 (2010) 390-394.
[54] M. Hakamada, T. Kuromura, Y. Chino, Y. Yamada, Y. Chen, H. Kusuda, M. Mabuchi, Monotonic and cyclic compressive properties of porous aluminum fabricated by spacer method, Mater. Sci. Eng. A 459 (2007) 286-293.
[55] B. Zettl, H. Mayer, S.E. Stanzl-Tschegg, H.P. Degischer, Fatigue properties of aluminium foams at high numbers of cycles, Mater. Sci. Eng. A 292 (2000) 1-7.
[56] B. Zettl, H. Mayer, S.E. Stanzl-Tschegg, Fatigue properties of Al–1Mg–0.6Si foam at low and ultrasonic frequencies, Int. J. Fatigue 23 (2001) 565-573.
[57] A. Kim, I. Kim, Effect of specimen aspect ratio on fatigue life of closed cell Al-Si-Ca alloy foam, Acta Mechanica Solida Sinica 21 (2008) 354-358.
[58] M. Kolluri, M. Mukherjee, F. Garcia-Moreno, J. Banhart, U. Ramamurty, Fatigue of a laterally constrained closed cell aluminum foam, Acta Mater. 56 (2008) 1114-1125.
[59] A.M. Harte, N.A. Fleck, M.F. Ashby, The fatigue strength of sandwich beams with an aluminium alloy foam core, Int. J. Fatigue 23 (2001) 499-507.
[60] O. Schultz, A. des Ligneris, O. Haider, P. Starke, Fatigue Behavior, Strength, and Failure of Aluminum Foam, Adv. Eng. Mater. 2 (2000) 215-218.
[61] L. Vendra, B. Neville, A. Rabiei, Fatigue in aluminum–steel and steel–steel composite foams, Mater. Sci. Eng. A 517 (2009) 146-153.
[62] H.M. Jaeger, S.R. Nagel, Physics of the Granular State, Science 5051 (1992) 1523-1531.
[63] S. Torquato, T.M. Truskett, P.G. Debenedetti, Is Random Close Packing of Spheres Well Defined?, Phys. Rev. Lett. 84 (2000) 2064-2067.

[64] I.N. Orbulov, J. Dobránszky, Producing metal matrix syntactic foams by pressure infiltration, Per. Pol. Mech. Eng. 52 (2008) 35-42.
[65] I.N. Orbulov, J. Ginsztler, Compressive characteristics of metal matrix syntactic foams, Composites Part A 43 (2012) 553-561.
[66] K. Májlinger, I.N. Orbulov, Characteristic compressive properties of hybrid metal matrix syntactic foams, Mater. Sci. Eng. A 606 (2014) 248-256.
[67] A. International, ASTM E739-10 (2015) Standard Practice for Statistical Analysis of Linear or Linearized Stress-Life (S-N) and Strain-Life (ε-N) Fatigue Data, ASTM International, West Conshohocken, PA, 2015.
[68] Y.-L. Lee, J. Pan, R. Hathaway, M. Barkey, Fatigue Testing and Analysis (Theory and Practice), Elsevier Butterworth-Heinemann, United States of America, 2005.
[69] K. Myers, B. Katona, P. Cortes, I.N. Orbulov, Quasi-static and high strain rate response of aluminum matrix syntactic foams under compression, Composites Part A 79 (2015) 82-91.
[70] C. Kádár, K. Máthis, I.N. Orbulov, F. Chmelík, Monitoring the failure mechanisms in metal matrix syntactic foams during compression by acoustic emission, Mater. Lett. 173 (2016) 31-34.
[71] D.D. Luong, O.M. Strbik III, V.H. Hammond, N. Gupta, K. Cho, Development of high performance lightweight aluminum alloy/SiC hollow sphere syntactic foams and compressive characterization at quasi-static and high strain rates, J. Alloys Compounds 550 (2013) 412-422.